Full length article

Microfluidic 3D platform to evaluate endothelial progenitor cell recruitment by bioactive materials

Adrián López-Canosa [a,b], Soledad Pérez-Amodio [a,b,c], Elisabeth Engel [c,a,b,*], Oscar Castaño [d,a,e,*]

[a] Biomaterials for Regenerative Therapies, Institute for Bioengineering of Catalonia (IBEC), The Barcelona Institute of Science and Technology (BIST), Baldiri i Reixac 10-12, Barcelona 08028, Spain
[b] CIBER en Bioingeniería, Biomateriales y Nanomedicina (CIBER-BBN), Madrid 28029, Spain
[c] IMEM-BRT Group, Department of Materials Science and Engineering, EEBE, Technical University of Catalonia (UPC), Barcelona 08019, Spain
[d] Electronics and Biomedical Engineering, Universitat de Barcelona (UB), Barcelona 08028, Spain
[e] Institute of Nanoscience and Nanotechnology, Universitat de Barcelona (UB), Barcelona 08028, Spain

ARTICLE INFO

ABSTRACT

Most of the conventional *in vitro* models to test biomaterial-driven vascularization are too simplistic to recapitulate the complex interactions taking place in the actual cell microenvironment, which results in a poor prediction of the *in vivo* performance of the material. However, during the last decade, cell culture models based on microfluidic technology have allowed attaining unprecedented levels of tissue biomimicry. In this work, we propose a microfluidic-based 3D model to evaluate the effect of bioactive biomaterials capable of releasing signaling cues (such as ions or proteins) in the recruitment of endogenous endothelial progenitor cells, a key step in the vascularization process. The usability of the platform is demonstrated using experimentally-validated finite element models and migration and proliferation studies with rat endothelial progenitor cells (rEPCs) and bone marrow-derived rat mesenchymal stromal cells (BM-rMSCs). As a proof of concept of biomaterial evaluation, the response of rEPCs to an electrospun composite made of polylactic acid with calcium phosphates nanoparticles (PLA+CaP) was compared in a co-culture microenvironment with BM-rMSC to a regular PLA control. Our results show a significantly higher rEPCs migration and the upregulation of several pro-inflammatory and proangiogenic proteins in the case of the PLA+CaP. The effects of osteopontin (OPN) on the rEPCs migratory response were also studied using this platform, suggesting its important role in mediating their recruitment to a calcium-rich microenvironment. This new tool could be applied to screen the capacity of a variety of bioactive scaffolds to induce vascularization and accelerate the preclinical testing of biomaterials.

Statement of significance

For many years researchers have used neovascularization models to evaluate bioactive biomaterials both *in vitro*, with low predictive results due to their poor biomimicry and minimal control over cell cues such as spatiotemporal biomolecule signaling, and *in vivo* models, presenting drawbacks such as being highly costly, time-consuming, poor human extrapolation, and ethically controversial. We describe a compact microphysiological platform designed for the evaluation of proangiogenesis in biomaterials through the quantification of the level of sprouting in a mimicked endothelium able to react to gradients of biomaterial-released signals in a fibrin-based extracellular matrix. This model is a useful tool to perform preclinical trustworthy studies in tissue regeneration and to better understand the different elements involved in the complex process of vascularization.

* Corresponding authors at: Biomaterials for Regenerative Therapies, Institute for Bioengineering of Catalonia (IBEC), The Barcelona Institute of Science and Technology (BIST), Baldiri i Reixac 10-12, Barcelona 08028, Spain; Electronics and Biomedical Engineering, Universitat de Barcelona (UB), Barcelona 08028, Spain
E-mail addresses: eengel@ibecbarcelona.eu (E. Engel), oscar.castano@ub.edu (O. Castaño).

1. Introduction

Bone defects are currently one of the major causes of disease worldwide due to the aging of the general population, which is as-

sociated with a dramatic increase in bone deterioration in terms of composition, structure, and function [1]. The most common approach to treating these conditions is the use of autologous grafts. However, this method faces many limitations such as the scarcity of healthy bone tissue at the donor site, high associated morbidity, or requiring complex surgeries [2,3]. A possibility to overcome some of these shortcomings is to use allogenic grafts, but they also pose other problems such as immunological rejection or infectious risks [4]. Therefore, during the last decades, extensive research has been performed to artificially synthesize biomaterials that meet the requirements of an effective bone substitute, such as being highly biocompatible or having excellent osteoconductive and osteoinductive properties [5,6].

Of the different developed materials, calcium phosphates (CaPs) are among the most widely used, as they fulfill all the aforementioned requirements due to their chemical similarity to the inorganic phase of the bone matrix [7]. Over the last decades, most of the research on calcium phosphates has focused on improving their osteogenic potential, often disregarding the crucial role of vascularization in the effective integration of the material [8]. Most strategies to stimulate vascularization have focused on adding biological agents to the materials, such as proteins or cells. In the first category, the most common approach is to use pro-angiogenic factors such as the vascular endothelial growth factor (VEGF) [9,10] or basic fibroblast growth factor (bFGF) [11,12]. This is an efficacious strategy but has several downsides such as the short half-life of the used proteins, the high production costs, and the complexity of delivering safe, effective, and therapeutic doses [13,14]. For this reason, there is an increasing interest in optimizing the physicochemical properties of the CaPs in order to be able to stimulate vascularization without the need for any additive. One of the most interesting approaches is to tune the release of calcium ions (Ca^{2+}) resulting from the dissolution products of CaPs. It has been shown that adequate levels of extracellular calcium are able to stimulate osteoinduction and osteogenesis in BM-rMSCs acting via the calcium-sensing receptor (CaSR), which is a G protein-coupled receptor expressed in different cell types that can detect calcium variations in the millimolar range [15,16]. It has also been observed that composites based on the combination of CaPs with polylactic acid (PLA) or ε-polycaprolactone (PCL) matrices can stimulate vascularization *in vivo* [17–19].

Current models to test the neovascularization of biomaterials pose many limitations to the understanding of the precise mechanisms at play. One of the most commonly used procedures is the chick embryo chorioallantoic membrane (CAM) assay, which is based on the implantation of the material or compound on the extraembryonic membrane of the developing chick egg [20]. One of the main problems of this model is the difficulty of decoupling the effects of the specific ions of interest from other CaP parameters such as the mechanical properties or the porosity, which have been demonstrated to strongly influence vessel formation [21–25]. These problems are also present in other *ex vivo* or *in vivo* assays, which also have other drawbacks such as being highly costly and time-consuming [26]. Traditional angiogenesis assays *in vitro*, on the other hand, have a low predictive power due to their poor biomimicry (lack of proper 3D structure for instance) and minimal control over many cell cues such as spatiotemporal biomolecule signaling [26]. Nevertheless, during the last decade, the advancements in microfabrication technologies have provided new platforms that allow the generation of cellular microenvironments that closely resemble the actual *in vivo* conditions, generally known as microphysiological systems or organs-on-a-chip [27,28]. Such systems are great tools to model angiogenesis [29–32], offering many advantages such as the precise control of the spatiotemporal cell microenvironment, compatibility with high-resolution imaging in real-time, or requiring smaller amounts of cells and reagents,

which translates into reduced costs. However, few research works have adopted microfluidic platforms as a tool to evaluate biomaterials [33,34].

In this work, we propose a microfluidic-based assay to study the effect of calcium-releasing biomaterials on endothelial progenitor cell recruitment. To achieve this goal, we designed, fabricated, and validated the capacity of the proposed microfluidic platform to generate gradients of soluble factors using a finite element model (FEM) of diffusion. We evaluated the suitability of the platform to study 3D migration to inorganic ions by evaluating the response of BM-rMSCs and rEPCs to gradients of calcium. We then implemented an assay to study the migratory response of rEPCs to calcium-releasing scaffolds in a co-culture microenvironment with BM-rMSCs. We also screened the release profile of several pro-angiogenic and inflammatory cytokines and performed an in-depth study of the role of osteopontin in mediating the response of rEPCs to high extracellular calcium levels. Overall, we believe that the presented microfluidic assay could be of great interest to performing preclinical studies with materials for bone tissue engineering and a better understanding of the different elements involved in the complex process of vascularization.

2. Materials and methods

2.1. Cell culture

Bone marrow-derived rat endothelial progenitor cells (rEPCs) and mesenchymal stromal cells (BM-rMSCs) were obtained from the long bones of young Lewis rats (2–4 weeks old) following previously published protocols [35,36]. Cells were isolated from different male animals and pooled together and cryopreserved. Briefly, the bone marrow was obtained from the rat's long bones by flushing adhesion medium M199 (Sigma, DE) supplemented with 20% fetal bovine serum, 1% pyruvate, 1% penicillin/streptomycin, 1% L-glutamine (all reagents from Thermo Fisher, US) and 22 μg/ml heparin (Sigma, DE). The whole fraction was plated in 6-well plates and incubated for 24 h. BM-rMSCs were the most adherent cells attached to the dish during this time and they were subsequently plated in T75 flasks (Thermo Fisher, US) and cultured in α-minimal essential medium (α-MEM) supplemented with 10% FBS, 1% Pen/Strep, and 1% L-glutamine (all reagents from Thermo Fisher, US) for no more than 5 passages. The initial plating density for BM-rMSCs was approximately $5.3 \cdot 10^3$ cells/cm^2. Cell phenotype was confirmed by positive staining for Stro1, CD105, and CD44, which are generally accepted markers for this lineage [37]. The osteogenic and adipogenic potential of isolated BM-rMSCs was confirmed by incubating the cells with osteogenic and adipogenic cell culture media

Cells in suspension were recovered and plated in new dishes for another 24 h. On the third day, the suspension fraction was highly enriched in hematopoietic cells, which were recovered and plated in T75 flasks and further cultured in Endogro media (Merck Millipore, DE) for no more than 5 passages. All cells were cultured in a humidified 5% CO_2 incubator at 37 °C.

All rEPCs used in this study were properly characterized as endothelial progenitor cells. Cells formed typical tube-like structures in the Matrigel assay after 4 h stimulation with 40 ng/ml VEGF and 24 h (data not shown). They also sprouted and formed tube-like structures when covered in collagen I gel for 3 days. Immunofluorescence staining demonstrated a majority of cells expressing Flk-1, weak CD31 and CD34, and diffuse vWF staining at passage 1. Ulex europaeus lectin binding was also positive. This phenotype was consistent with an immature, endothelial-like progenitor state as described by others [37–39]. Flow cytometry for CD45 and CD11b was performed on passage 4 cells to assess the purity of the population studied. Results showed a small proportion of cells express-
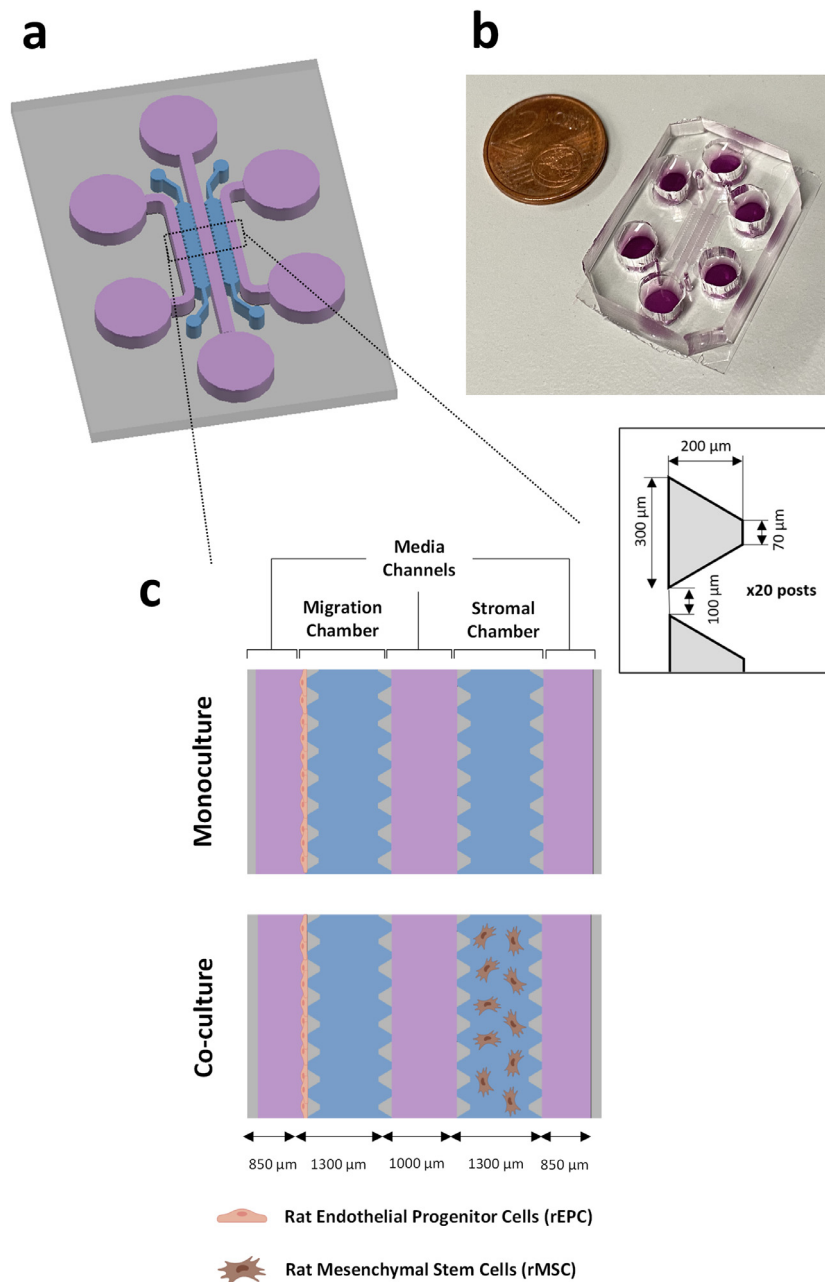
Fig. 1. Microfluidic assay to study rEPC recruitment. (a) Scheme of the device showing the 2 cell chambers (blue) and the media channels (purple). (b) Picture featuring the final assembled platform. (c) Comprehensive view detailing how cells are cultured in the device, either in monoculture (just one cell type, migration caused by the addition of a chemoattractant to the cell media) or co-culture conditions (two cell types, migration induced by the secretions of the cells located in the stromal cell chamber).

ing hematopoietic markers (2.12% positive for CD45 and 2.19% for CD11b), confirming very low hematopoietic contamination in regular cultures. All these results were reported previously by our group [40].

2.2. Device design and fabrication

The design of the microfluidic platform (see Fig. 1-a,b) was performed using computer-aided design software (Auto-CAD 2019, Autodesk, US) and consists of 2 cell culture chambers (1300 µm x 8800 µm x 150 µm) in contact with 2 cell culture media channels (750 µm wide, 150 µm high) separated among them by a central channel (1000 µm wide, 150 µm high). Master molds were produced using photolithography with a SU8–3050 photoresist (MicroChem, DE) and 4'' Si wafers as supports. All pro-

cedures were performed in a cleanroom environment (see supplementary data). Polydimethylsiloxane elastomer (PDMS, Sylgard 184, Dow Corning) was used at 10:1 w/w (base: curing agent). After degassing and curing overnight at 65 °C, the PDMS was carefully removed from the silicon wafer, separated into individual chips, and perforated producing 6 mm holes for reservoirs and 1 mm holes for chamber inlets. Chips were cleaned and bonded to glass rectangular supports (0.17 mm thick coverslips) by oxygen plasma treatment (Harrick Plasma PCD-002-CE) for 0.5 min at 10.5 W. In the case of biomaterial testing, the used coverslips were patterned with PLA nanofibers (more details in methods Section 2.4), and fibers outside the stromal cell chamber area were carefully removed before the plasma treatment with a cloth wetted in acetone (Panreac, ES). Finally, all the chips were cured at 85 °C for 12 h to strengthen the bonding. Devices were sterilized by placing them in

the plasma chamber and repeating the previously described process.

2.3. Finite element model of protein transport and validation

An *in silico* model of the device was developed using the finite element method (FEM) to evaluate if a concentration gradient could be obtained in the migration chamber from the secretions produced by the BM-rMSCs. The creation of such a gradient is based on the passive diffusion of the protein of interest through the porous hydrogel (fibrin) injected in the cell chamber area (migratory chamber). To study the diffusive process, the geometry of the platform was split into two domains with different diffusive properties: (1) the fluid area associated with the cell media, including the channels and reservoirs, and (2) the cell chambers filled with fibrin hydrogel. The concentration profile was calculated with COMSOL Multiphysics 5.6 (COMSOL Inc, US) using the *Transport of Diluted Species* interface, which in our particular case solves the mass conservation equation considering that there is no convective transport involved. This yields an equation corresponding to Fick's laws of diffusion:

$$J_i = -D\nabla c$$

$$\frac{\partial c}{\partial t} = \nabla J_i + R$$

Where J_i (mol m^{-2} s^{-1}), is the diffusive molar flux vector, which evaluates the amount of substance that flows through a unit of the area during a unit time interval, c (mol m^{-3}) is the concentration of the chemical species of interest, D (m^2 s^{-1}) the diffusion coefficient and R (mol m^{-3} s^{-1}) the reaction rate of the considered species. A no flux boundary condition was selected for all walls of the system. A tetrahedral mesh with approximately 215,000 elements was used and solved based on the PARDISO approach. The reliability of the results was controlled by different mesh sensitivity processes.

In our case, we were interested in studying the diffusion of the osteopontin protein, which has an approximate molecular weight of 31 kDa, that is in the range of other well-known angiogenic factors such as VEGF, bFGF, or IGF [41]. The diffusion coefficient for molecules with that hydrodynamic radius is around 6×10^{-11} m^2/s in cell media and 4.9×10^{-11} m^2 s^{-1} in hydrogels such as collagen or fibrin [42,43]. The osteopontin secretion on day 3 was derived from an ELISA assay performed on BM-rMSCs (see methods Section 2.8) and estimated to be approximately 1.41×10^{-12} mol m^{-3} s^{-1} (assuming a linear release profile).

To validate the computational model, we studied the concentration profile of a 40 kDa Texas Red conjugated dextran (Thermo Fisher, US), a non-reactive polymer with a comparable hydrodynamic radius to osteopontin. To perform the experiment, both cell chambers were loaded with the fibrin gel (2.5 mg/ml fibrinogen and 1 U/ml thrombin), one of the side channels filled with regular PBS and the remaining two with a solution of fluorescent dextran in PBS at an initial concentration of 25 μg ml^{-1}. Fluorescent images were acquired in a Leica AF7000 microscope (Leica Systems, DE) at different time points (2.5, 5, 10, and 15 h) and images were processed with ImageJ software (NIH, US) to obtain the evolution of the fluorescent intensity profile. The area selected is located between the rows of posts 10 and 11 and the values were normalized using the intensity measurements from the fluorescent channel (maximum) and control channel (minimum). These results were compared to the values obtained in the finite element simulations (removing the reaction rate term), which were also normalized to allow for direct comparison.

2.4. Calcium-releasing biomaterial fabrication

The calcium-releasing biomaterial chosen for evaluation in our platform was based on CaP ormoglass nanoparticles (NP) prepared using a sol-gel process and the CaO:P$_2$O$_5$:Na$_2$O:TiO$_2$ 44.5:44.5:6:5 molar ratio composition reported by Sanzana et al. [44]. After obtaining the NP, they were resuspended at 25% w/w (PLA+NP25) by ultrasonic dispersion in 4% w/w poly-L/DL lactic acid solution (Purasorb PLDL 7038, 70/30 L-lactide/DL-lactide copolymer, inherent viscosity midpoint 3.8 dl g^{-1}, molecular mass ≈ 850,000 Da, Corbion, NL) in 2,2,2-trifluoroethanol (TFE, 99% Alfa Aesar, US). The plain PLA 70/30 solution was used to produce the control PLA fibers. 5 ml syringes (Becton-Dickinson, US) were loaded with the polymer solutions and pumped (NE-300, New Era Inc, USA) at a flow rate of 1 ml/h through a 21-gage blunt-tip needle (Nordson EFD, US). A high-voltage power supply (NanoNC, KR) was used and fibers were collected onto a grounded cylindric collector located at 200 mm from the tip of the syringe. Rectangular fragments of aluminum foil (20 × 33 cm) were used to envelop the collector. Three 0.17 mm coverslips (Deltalab, ES) were secured with adhesive tape following the middle axis of the aluminum foil rectangle. A rotary speed of 1000 rpm was used to obtain aligned fibers. The deposition time was 10 min and the applied voltage was 15 kV.

Several properties of the material have been compiled in Table S1.

2.5. Biomaterial morphology and Ca^{2+} release characterization

The calcium ions release profile of the PLA+NP25 was measured by preparing three electrospun coverslips and bonding them to a PDMS block (7 mm in height). A custom-made device based on a PDMS block with a 10 mm punch hole in the middle of the block, previously removing most of the fibers outside the punched area as explained in the previous section. 500 μl of culture media obtained mixing α-MEM and Endogro media at 1:1 (more details in Section 2.5) were added to each device. Samples were kept inside 100 mm Petri dishes in a 5% CO$_2$ incubator at 37ºC and the medium was replaced at different time points for a total period of 48 h. The calcium concentration of each replaced medium was obtained using the O−Cresophtalein complexone assay and measuring the absorbance of the samples using an Infinite M200 Pro-plate reader (Tecan, CH). The shape of the fibers, previously coated with gold was featured using scanning electron microscopy with an electron source by field emission (NOVA Nano SEM 230, Fei Co., NL) at 10 kV.

2.6. Migration assays

Cells were seeded in the microfluidic system either in monoculture or co-culture conditions (see Fig. 1-c). In the first case, both cell chambers were loaded with a fibrin gel obtained by mixing a fibrinogen solution at 2.5 mg/ml with 1 U/ml of thrombin (both reagents from Sigma, DE). In the co-culture experiments, the migration chamber was loaded with acellular fibrin and the stromal one with a solution consisting of 10 × 10^6 cells ml^{-1}, either resuspended in a fibrin gel (10 μl) or directly seeded on top of the electrospun fibers. The devices were either incubated at 37 ºC for 15 min to allow for hydrogel polymerization or 1 h to allow BM-rMSCs to attach to the PLA fibers. The cells (just rEPCs in the case of co-culture conditions) were centrifuged and resuspended at a concentration of 1 × 10^6 cells ml^{-1} and seeded in the device by putting 50 μl in the upstream reservoir of one of the side channels and aspirating from the other end. The devices were then tilted 90º and incubated for 45 min to allow for cell attachment.

In the case of the monoculture experiments, all reservoirs were filled with the regular cell media (approximately 150 μl/reservoir)

and kept for 1 day under those conditions. During the next 2 days, the devices were either kept without supplementation or mixed with VEGF (Preprotech, US) at 100 ng ml^{-1} or CaCl$_2$ (Sigma, DE) at 10 mM in the acellular channels. The media was changed every 15 h in order to reset the concentration gradient in the migration chamber. In the co-culture experiments, the media of both cell populations was mixed at a 1:1 ratio, used during day 1 without supplementation (control) and for the next 2 days either in control conditions, supplemented with CaCl$_2$ at 10 mM or supplemented with CaCl$_2$ plus osteopontin neutralizing antibody (Human Osteopontin/OPN Antibody (AF1433SP), R&D Systems, MN, US) at 10 µg/ml. No changes of media were performed to avoid disrupting the gradient generated by the BM-rMSCs secretions. For biomaterial testing, no supplementation was used. In all cases, low serum (2% FBS) conditions were considered. Each device was kept inside 100 mm Petri dishes in a 5% CO$_2$ incubator at 37ºC. Three replicates were performed per experimental condition.

2.7. Immunostaining and cell migration quantification

The cells seeded in our microfluidic platform were fixed after 72 h in culture with 4% paraformaldehyde (Electron Microscopy Sciences, US) for 15 min after removing unreacted paraformaldehyde with sterile 1x PBS. After another 1x PBS washing, they were permeabilized with a Triton X-100 (Sigma, DE) solution at 0.1% v/v in 1x PBS with glycine (Sigma, DE) at 0.15% w/v (PBS-gly) for 15 min. Then, cells were stained by incubating them at room temperature for 2 h with a rhodamine-phalloidin (Thermo Fisher, US) solution at 1:200 in PBS-gly. A counterstaining for cell nuclei were also implemented by incubating 4′,6-diamidino-2-phenylindole (DAPI, Thermo Fisher, US) at 1:1000 in PBS-gly for 10 min at room temperature. Samples were then washed three times in PBS-gly and maintained at 4ºC in the same solution until acquisition.

Imaging was performed on a TCS SP-5 confocal microscope (Leica Microsystems, DE). Cell migration was quantified with a custom-made procedure using the software Image J-Fiji [45]. Briefly, the acquired images were projected as a z-stack (maximum intensity) and a reference line was drawn at half the microposts width (using the bright field channel) in order not to take into account any basal cell invasion of the gel. Then, the cartesian coordinates and the total number of migrated cells were automatically calculated from the DAPI channel using the *3D Objects Counter* plugin [46]. The migrated distance of each cell was calculated as the difference between the x-coordinates (or y-coordinates depending on how the chip was placed) and corresponding coordinates of the reference line at half the microposts width. One representative image in the middle of the cell chamber (between rows 10 and 11) was taken per chip from a total of 3 replicates in any experimental condition. Cell number was quantified only from the selected area.

2.8. Proliferation and protein secretion assays

To perform the proliferation assay, 10×10^6 cells ml^{-1} were seeded in the stromal chamber and resuspended in fibrin gel (10 µl) as previously explained. The rest of the device was filled either with control media or media supplemented with CaCl$_2$ at 10 mM (150 µl/reservoir). Cells were kept in culture for 3 days with a change of media after day 1. Proliferation was quantified by measuring the ratio of dsDNA in cell lysates using the PicoGreen kit at two-time points: 3 h after the initial seeding (to get an estimate of the initial amount of dsDNA) and after 3 days in culture. To obtain the lysates, cells were recovered from the devices after dissolving the fibrin gel by incubating with TrypLE (Thermo Fisher, US) for 45 min at 37 ºC in agitation. The cells were then centrifuged and

resuspended in 300 µl of Tris-EDTA (Sigma, DE) and lysed by subjecting them to three freeze-thaw cycles. The PicoGreen assay was then performed following the manufacturer's instructions. Fluorescence measurements were performed in an Infinite M200 Pro-plate reader (Tecan, CH). Three replicates were performed per condition and time point.

The conditioned media collected on day 3 from the devices seeded with 3D BM-rMSC monoculture was used to measure the amount of OPN released by the cells. We also analyzed the conditioned media obtained on day 3 from BM-rMSC monocultures seeded on top of the biomaterials for several pro-angiogenic and inflammatory proteins (IL-1β, IL-6, OPN, IGF-2). In both cases, protein secretion was analyzed using an ELISA kit (Rat IL-1β/IL-1F2 Quantikine ELISA Kit (RLB00); Rat IL-6 Quantikine ELISA Kit (R6000B); R&D kit Quantikine ELISA for Mouse/Rat osteopontin (MOST00); Mouse/Rat/Porcine/Canine IGF-II Quantikine ELISA Kit (MG200), R&D Systems, MN, US) following the manufacturer's instructions Absorbance measurements were performed in an Infinite M200 Pro-plate reader (Tecan, CH). The absorbance measurements of each sample were corrected by subtracting the baseline signal corresponding to the regular cell culture media to account for the basal presence of some of the analyzed proteins. The final values were also normalized with respect to the amount of dsDNA obtained for each of the samples. Three replicates were performed per experimental condition.

2.9. Statistical analysis

Prism 8.3 software (GraphPad Software, US) was used to statistically treat all generated data., which was tested for normality and presented and analyzed with the mean and the standard deviation or the median and the quartile. For 2 samples comparison, Student's *t*-test (unpaired, two-tailed distribution) was used, while for the multiple samples (unless otherwise specified) comparison with a one-way ANOVA was followed by a post-hoc Tukey's test. Statistical significance was considered from *p*-value < 0.05 (*).

3. Results and discussion

3.1. A microfluidic platform allows the generation of 3D protein gradients

To demonstrate the possibility of generating a protein gradient inside the proposed microfluidic platform, we created and validated a finite element model of the device for the transport of diluted species using a 40 kDa dextran. We chose this molecular weight because its diffusion coefficient is really close to that of several pro-angiogenic proteins such as VEGF, representing a diffusivity analog of those molecules [31,41,43]. We compared the simulation results with the experimental values for different time points in a total interval of 15 h (see Fig. 2-a). It can be observed that the gradient becomes linear after approximately 2.5 h, with a progressive increase of the dextran concentration in the control channel from 0 to 0.125 µM (approximately 25% of the maximum concentration), which can be reset by changing the media as previously explained in Section 2.6. The average slope obtained in the finite element model when the gradient becomes linear (2.77 $\times$ 10^{-4} µM µm^{-1}) and the experimental one (2.88 $\times$ 10^{-4} µM µm^{-1}) are not significantly different ($p > 0.005$), which indicates that the computational model is able to adequately predict the behavior of our system. It is important to highlight that protein binding to the gel, as well as blocking and consuming mechanisms related to the rEPC monolayer, were neglected in order to perform the comparisons. This means that the dextran profile does not exactly mimic the real protein gradient, although it gives us important insight into the diffusion mechanisms in our system.
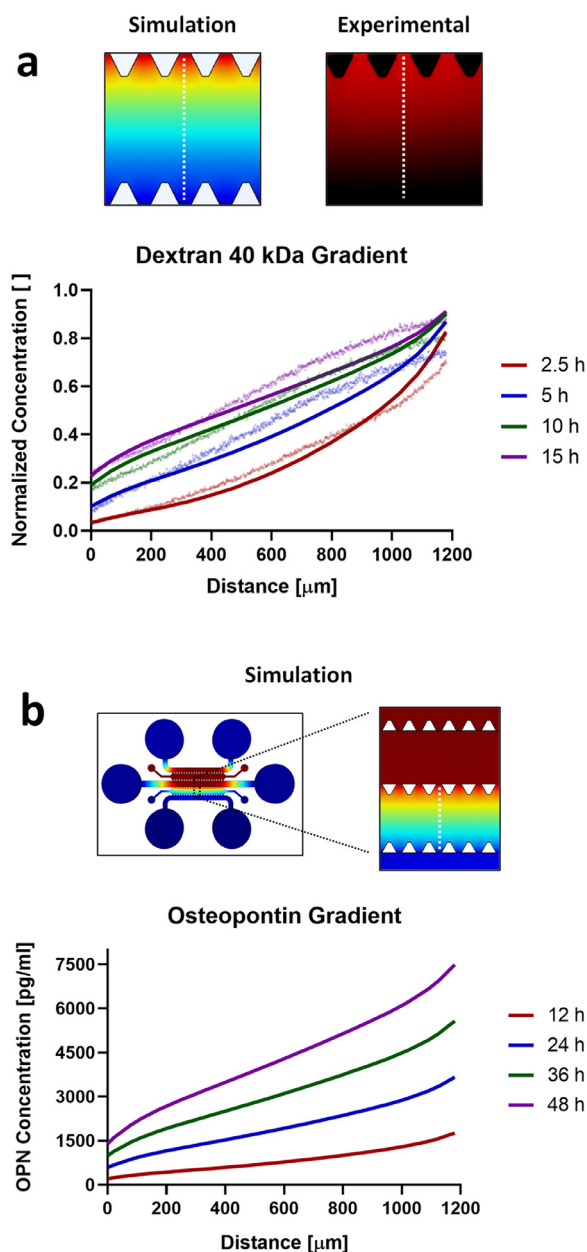
Fig. 2. Finite element model of protein diffusion in microfluidic platform. (a) Comparison of the normalized concentration gradients obtained in the FEM simulations (solid lines) with the experimental fluorescence measurements (dotted lines) for different timepoints. (b) Computational model of the gradients generated by the BM-rMSC osteopontin secretions in the migration chamber for different timepoints. In both cases, the gradient profile corresponds to a transversal section of the cell chamber between rows of posts 10 and 11.

For the monoculture conditions, results obtained for the dextran experiments suggest that applying the VEGF at a concentration of 100 ng ml^{-1} would yield a linear gradient after about 2.5 h with an average slope of approximately 55 ng ml^{-1} that can be maintained for at least 12 h. In the case of Ca^{2+}, it has been demonstrated that simple ions can freely diffuse in the high water content of the hydrogel [47], which implies that the gradient dissipates much faster. In fact, our simulations (see Fig. S1) show that the calcium gradient dissipates over 1 h. However, the results presented in Section 3.2 evidenced that this time interval is enough to activate cell migration. In the case of co-culture conditions, we utilized the finite element simulation to address how OPN gradient could be generated from the stromal chamber into the mi-

gration chamber. The results show (see Fig. 2-b) that linear gradients are generated with increasingly steeper slopes with the time in culture. For instance, after 24 h the gradient is 2.36 ng ml^{-1} mm^{-1}, increasing to 4.70 ng ml^{-1} mm^{-1} after 48 h. These results are in the range of previously reported studies with encapsulated human lung fibroblasts (hLF) [48], suggesting that the dimensions of the device allow paracrine communication between rEPCs and BM-rMSCs.

3.2. Validation of the microfluidic platform to study chemotaxis and proliferation of BM-rMSCs and rEPCs

After evaluating the diffusive transport of bioactive molecules in our device, we performed several assays to demonstrate that the platform can be used to study the migration and proliferation of the cells of interest and evaluate the effects of calcium in their recruitment. Our results (see Fig. 3-a,b) show that the creation of a calcium gradient in the migratory chamber is able to elicit a strong chemotactic response in BM-rMSCs in 3D, with a mean migrated distance of 124.7 ± 14.7 μm with respect to half of the microposts width (dashed line in Fig. 3-a). This response is comparable to the one obtained using VEGF at 100 ng ml^{-1} (129.3 ± 6.7 μm), a growth factor that has been demonstrated to induce MSCs' mobilization via ERK- and FAK-depending pathways [49]. In both cases, the migratory response is significantly higher than the control, in which the cells remain adhered to the wall without invading the gel. This data suggests that the transient calcium gradient, despite dissipating quickly, is enough to activate cell migration. The mean number of migrated cells is 28 ± 7 for CaCl$_2$ and 32 ± 5 for VEGF, which reinforces the idea of their chemotactic potential. The dsDNA quantification shows an almost two-fold increase in cell proliferation (see Fig. 3-c), which probably shows that after the induction of BM-rMSCs' migration starts the proliferation, as a process involved in physiological or pathological conditions such as the development of vasculogenesis/angiogenesis [50]. The obtained results seem to be in good agreement with previous experiments performed in 2D using Transwells, in which extracellular calcium also elicited a strong chemotactic response on these cells [36,51].

Regarding rEPCs, our results (see Fig. 4-a,b) show that the mean migrated distance when cells are subjected to the transient calcium gradient (60.3 ± 13.6 μm) is not significantly higher than that obtained for the control conditions (49.0 ± 10.0 μm). However, when the gradient is generated using VEGF at 100 ng/ml (which is widely known to potently stimulate endothelial cells mobilization), the migrated distance (107.7 ± 3.6 μm) is significantly higher than in the aforementioned conditions. The mean number of migrated cells is 12 ± 5 for the control condition, 10 ± 2 for the CaCl$_2$, and 37 ± 10 for the VEGF. These results agree with the proliferation data obtained by dsDNA quantification (see Fig. 4-c), as no significant differences were observed in calcium-treated media concerning the control condition. In this case, the obtained results are in contrast with previous 2D assays, in which a significant increase in chemotaxis was reported [17,35]. We believe that the observed differences can be due to the limitations related to 2D assays, such as the lack of 3D architecture or the use of thin artificial 2D polycarbonate membranes that poorly resemble the native extracellular matrix (ECM) [52]. It is important to highlight that we did not quantify the dsDNA for cell proliferation in the case of the VEGF because it is a well-known inducer of mitosis and proliferation of these cell types [53,54]. Previously presented microfluidic systems with similar architectures have demonstrated their superior performance to Transwells to study processes like cell migration or angiogenesis [29,32,55], as they allow to better control of the biophysical and biochemical microenvironment as well as offer the possibility to incorporate perfusion and monitor cell migration in
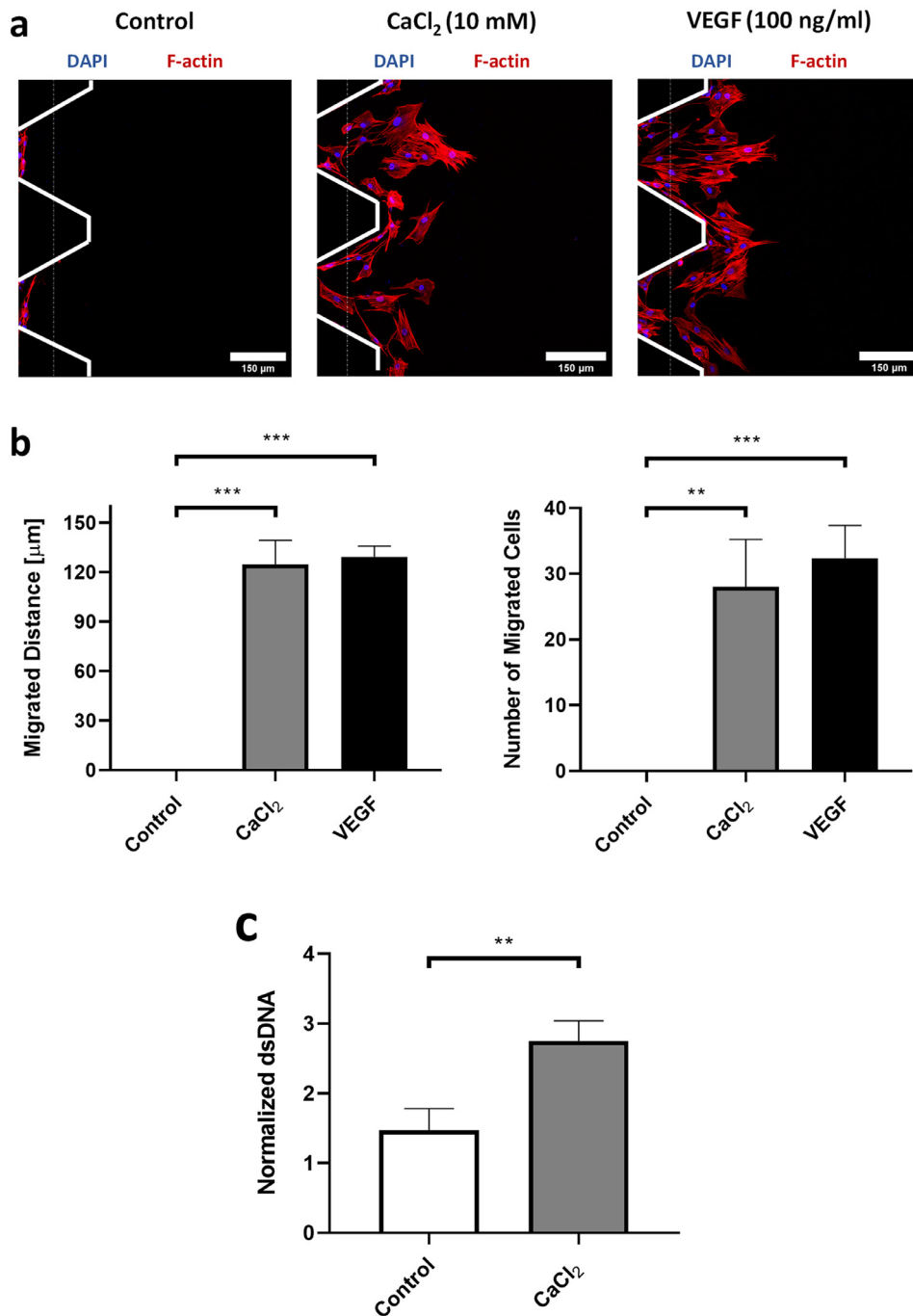
Fig. 3. Evaluation of migration and proliferation of BM-rMSC in 3D microfluidic assay. (a) Confocal images of BM-rMSC migration in three conditions: media with no supplementation (control), media supplemented with $CaCl_2$ at 10 mM and media with VEGF at 100 ng/ml. Cells were stained for F-actin (red), and cell nuclei (blue) after a total of 3 days in culture. (b) Analysis of the mean migrated distance and mean number of migrated cells with respect to the half of the microposts width (dotted white line in the microscopy images). (c) Proliferation index from the whole BM-rMSC 3D culture in the microfluidic devices. This index was obtained as the ratio of the dsDNA content of all the cells after 3 days in culture with respect to the initial amount. Results are expressed as mean $\pm$ standard deviation ($n = 3$) with $^*p < 0.05$, $^{**}p < 0.01$ and $^*p < 0.001$ (evaluated with Student's *t*-test).

real-time cell instead of relying only on end-point measurements [56].

Notice that migration assays on 2D culture plates or glass are usually not longer than 24 h. Our previous experiments showed low viability when they were conducted for up to 3 days. A concentration of 2% of serum was used in order to maintain cell viability for several days. We considered that some proteins and growth factors might be present in very low concentrations, but the same amount of serum was used in all conditions. We assumed that op-

timal conditions are serum-free, but in our case, after optimization, a reduced serum of 2% was needed for conducting the experiments.

3.3. Calcium-releasing PLA scaffolds significantly increase rEPCs recruitment compared to PLA controls in 3D microfluidic assay

Based on these previous results, we decided to assess the capacity of our platform to predict the recruitment of rEPCs using
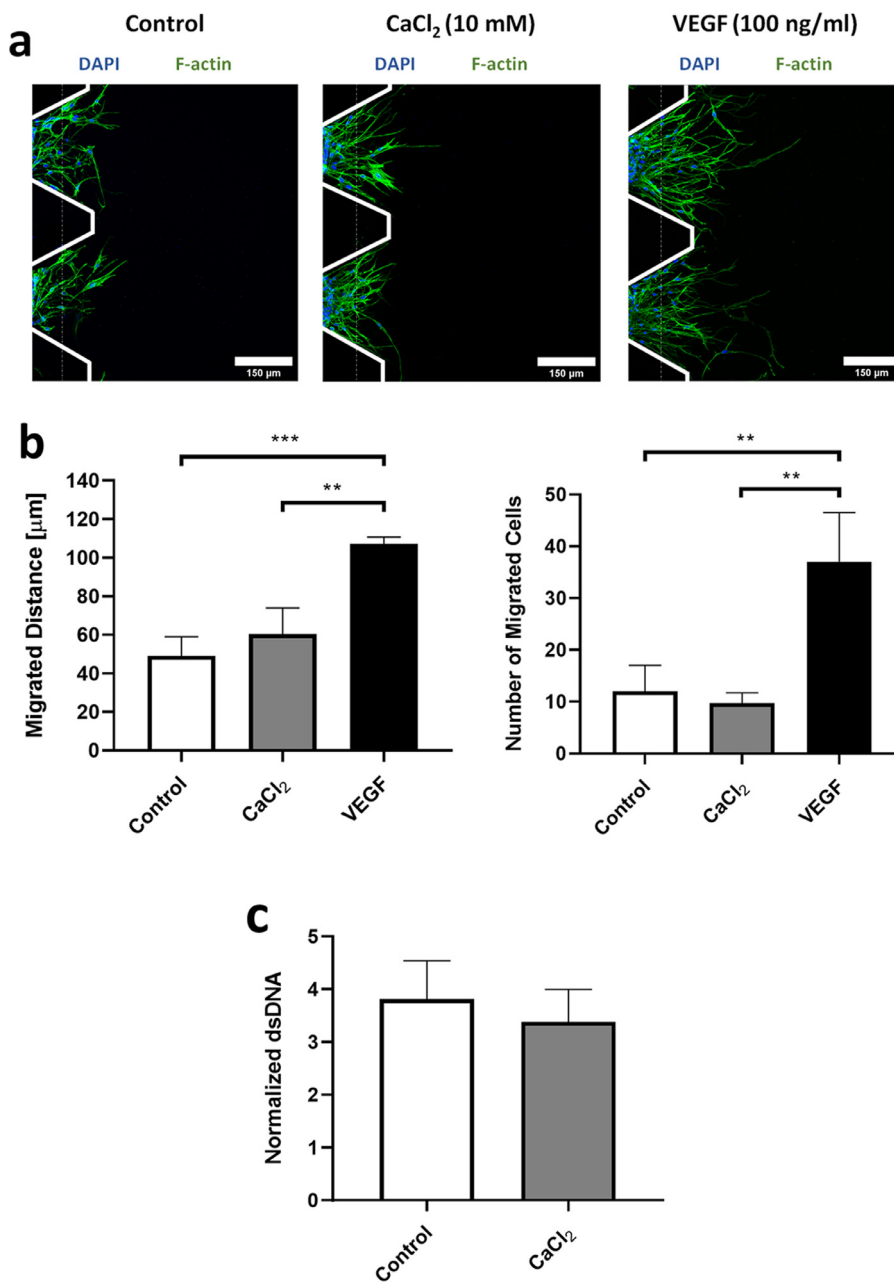
Fig. 4. Evaluation of migration and proliferation of rEPC in 3D microfluidic assay. (a) Confocal images of rEPC migration in three conditions: media with no supplementation (control), media supplemented with $CaCl_2$ at 10 mM and media supplemented with VEGF at 100 ng/ml. Cells were stained for F-actin (green), and cell nuclei (blue) after a total of 3 days in culture. (b) Analysis of the mean migrated distance and mean number of migrated cells with respect to the half of the microposts width (dotted white line in the microscopy images). (c) Proliferation index from the whole rEPC 3D culture in the microfluidic devices. This index was obtained as the ratio of the dsDNA content of all the cells after 3 days in culture with respect to the initial amount. Results are expressed as mean $\pm$ standard deviation ($n = 3$) with $^*p < 0.05$, $^{**}p < 0.01$ and $^*p < 0.001$ (evaluated with Student's *t*-test).

calcium-releasing biomaterials. To do so, we compared an electrospun composite scaffold made of PLA with calcium phosphate nanoparticles with PLA controls (no calcium release). The chosen composite has been shown to induce a significant increase in vascularization compared to regular PLA in a subcutaneous mice model [18]. In those experiments, the optimal range of nanoparticle loading was established between 20 and 30% (w/w), so we chose a ratio of 25% (PLA+NP25) for our experiments. Several relevant properties of the materials can be found in Table S1.

To perform the assay, we electrospun the biomaterials in the stromal chamber (see Fig. 5-a) and then seeded BM-rMSCs on top of the fibers to better recapitulate the bone microenvironment (see Fig. 6-a). In our study, we focused on paracrine signaling. Indeed,

it has been shown that, in co-culture conditions where the different cell types are in direct contact, MSCs tend to wrap around the endothelial cells and differentiate into mural cells (mainly pericytes) [57,58]. We characterized the morphology of the fibers using SEM imaging (see Fig. 5-b), which showed some differences in their arrangement, probably due to the formation of nanoparticle aggregates, which tend to induce a higher degree of disorder in the PLA+NP25 fibers. The cumulative calcium release profile in cell media (see Fig. 5-c) was also evaluated, yielding a basal level of around 1.5 mM in the PLA controls, which corresponds to the amount of $CaCl_2$ already present in most cells culture media formulations. In the case of the PLA+NP25, the peak in the instantaneous release occurs between 3 and 4 h after immersion, while
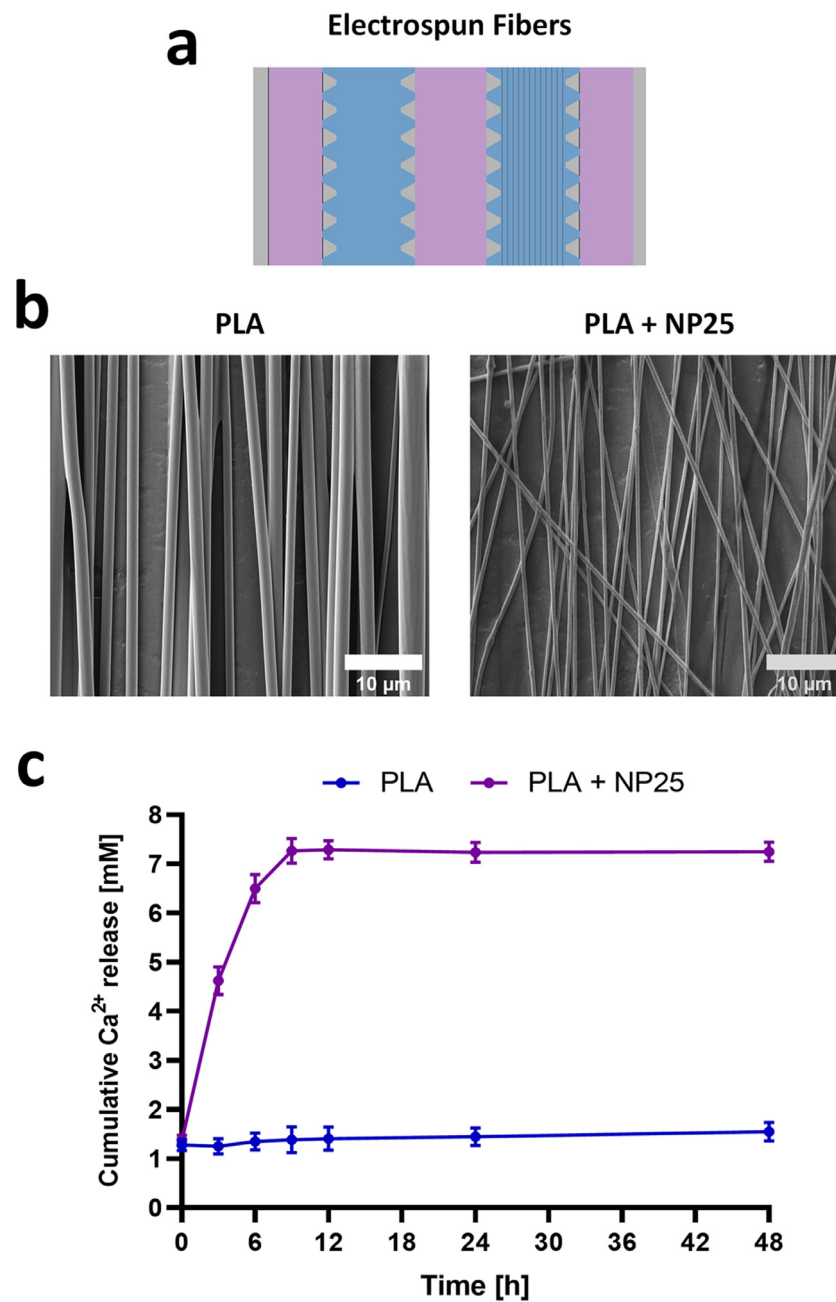
Fig. 5. Biomaterial characterization. (a) Schematic representation of the electrospun fibers deposition in the stromal chamber of our device. (b) FESEM pictures showing the electrospun fibers morphology, respectively. (c) Cumulative calcium release for the PLA fibers with CaP nanoparticles vs a regular PLA control for different timepoints (0, 3, 6, 9, 12, 24 and 48 h). Results are expressed as mean ± standard deviation ($n = 3$).

the cumulative amount of calcium reaches a maximum value of 7.25 ± 0.19 mM in around 10 h.

Notice that the calcium release of the scaffolds was measured using a custom-made device based on a PDMS block with a 10 mm punch hole in the middle in which the nanofibers were deposited. The total volume of culture media used in these experiments was 500 µl. We considered that the dimensions of the microfluidic devices could not have a huge influence on the release profile of the nanofibers, as the amount of total media volume used in the chips is in the same order ($\approx$500–600 µl) and the calcium diffuses really fast in the cell culture media (order of magnitude of 10^{-9} m^2/s).

Regarding rEPCs' migration (see Fig. 6-c,d), we observed a significantly higher migration in the case of PLA+NP25 with respect to the pure PLA controls, both in terms of the mean migrated dis-

tance (92.3 ± 5.0 µm vs 69.3 ± 11.2 µm) and the mean number of migrated cells (46 ± 13 vs 12 ± 3). As previously shown, calcium *per se* does not affect rEPCs' recruitment, so we checked for the release profile of a range of relevant pro-angiogenic and inflammatory proteins in BM-rMSC monocultures seeded on top of the two different materials. We could observe a significant increase in the release of IL-1β ($p \leq 0.01$), IL-6 ($p \leq 0.001$), IGF-2 ($p \leq 0.05$), and OPN ($p \leq 0.01$) in the case of the PLA+NP25 in our 3D microfluidic assay (see Fig. 6-b). We chose these proteins because some studies have reported that the use of elevated extracellular calcium caused an upregulation of some angiogenic genes such as those encoding insulin-like growth factors (IGF) [59]. Proinflammatory cytokines such as IL-1β or IL-6 have also been associated with scaffold vascularization processes. They cause the acti-
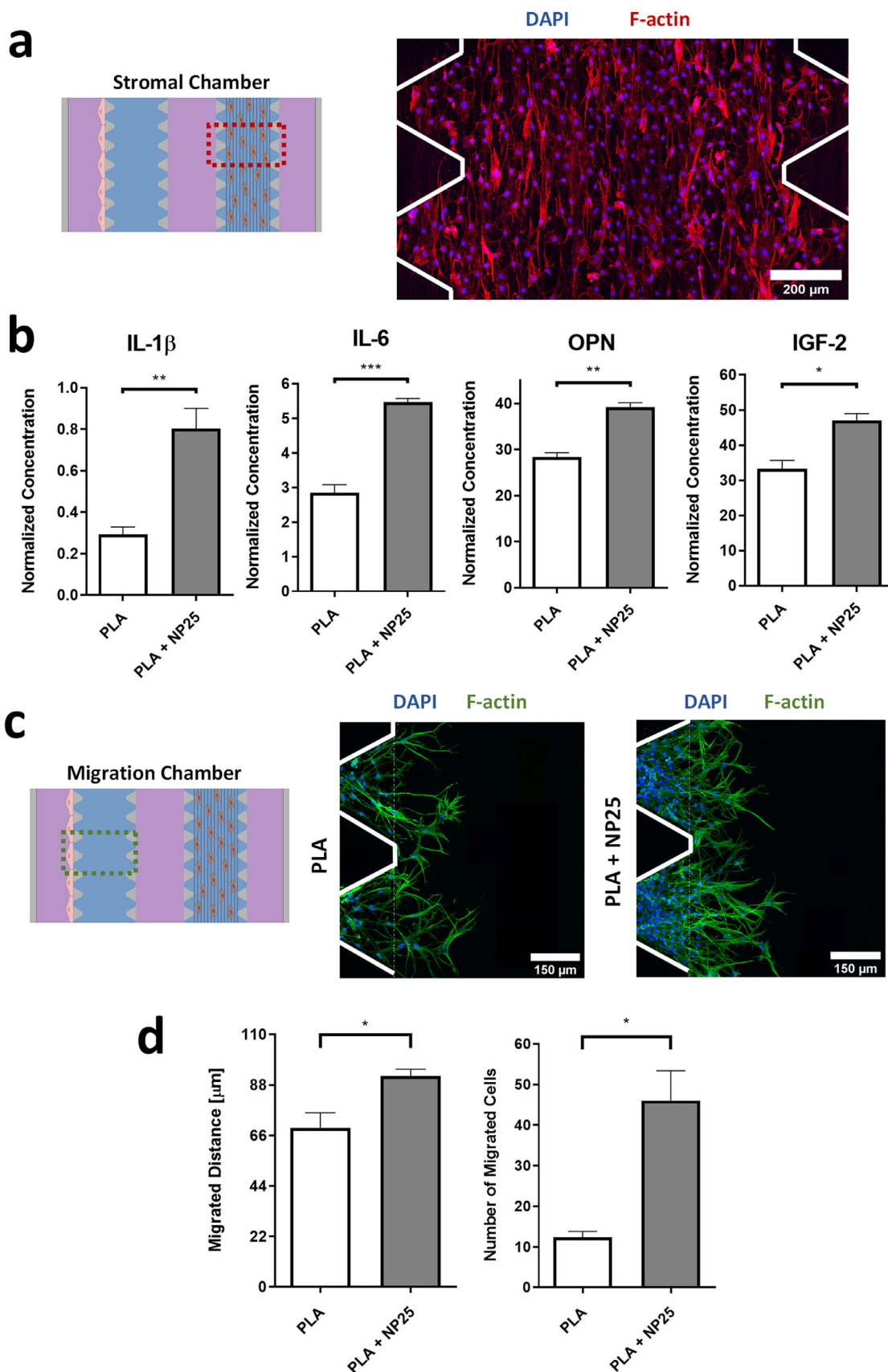
Fig. 6. Evaluation of the biomaterial effects on rEPC and BM-rMSC in 3D microfluidic assay. (a) Schematic of the seeding conditions for the BM-rMSC in the stromal chamber on top of the electrospun fibers and confocal image of the actual seeded cells stained for F-actin (red), and cell nuclei (blue) after a total of 3 days in culture. (b) Total release of different pro-angiogenic and inflammatory cytokines (IL-1β, IL-6, OPN, IGF-2) in cell media by BM-rMSC for 3 days. (c) Schematic of the migration experiment with rEPC in co-culture conditions with the biomaterial and confocal microscopy images for PLA fiber with the CaP nanoparticles at 25% w/w vs the regular control. Cells were stained for F-actin (green) and cell nuclei (blue) after a total of 3 days in culture. (d) Analysis of the mean migrated distance and mean number of migrated cells with respect to the half of the microposts width (dotted white line in the microscopy images). Results are presented as mean $\pm$ standard deviation ($n = 3$) with *$p < 0.05$ (Student's t-test).

vation of the M1 macrophages phenotype, which secrete high levels of angiogenic growth factors (such as VEGF) and metalloproteases involved in vascular remodeling. Osteopontin, a phosphorylated acidic RGD containing glycoprotein, was also considered in our analysis, as it is a prominent constituent of the bone matrix [36,55,60] that has been associated with angiogenesis in tumor microenvironments [61].

To the best of our knowledge, few studies have addressed the study of biomaterials using microfluidic platforms so far. One of these works is focused on evaluating hyaluronic acid-based hydrogels by studying the resulting networks formed by the self-assembling of human-induced pluripotent stem cell-derived endothelial cells (hiPSC-ECs) [33]. The main drawback of this platform is that its applicability is limited to the evaluation of vasculogenesis in hydrogel-based materials, as performing migration studies or incorporating rigid scaffolds is not possible in the proposed device. Another recent study has also put forward a microfluidic platform to evaluate expanded polytetrafluoroethylene (ePTFE) membranes by assessing the capacity of a preformed vascular network composed of human umbilical vein endothelial cells (HUVEC) and human lung fibroblasts (hLF) to colonize it [34]. However, although being an excellent proof of concept showing how microfluidics can be used to test biomaterials, we consider that there are some drawbacks that limit its applicability, especially for bone tissue engineering applications. For instance, it relies on a complex fabrication process requiring specialized laser cutting equipment and the creation of U-shaped pieces to fit the membrane in the device, which can lead to problems of gap formation between the substrate and the membrane. Moreover, the direct growth of the cells in the material makes it difficult to discern the different variables at play (bioactive ion release, porosity, etc.). We believe that our platform offers a low-cost and more robust solution for the study of the experimental variables independently, something that is not achievable with the aforementioned microfluidic assays or other commonly used *ex vivo* or *in vivo* assays such as the CAM assay [62], as it allows for the direct incorporation of the biomaterial scaffold (such as electrospun ones) without direct cell contact to study the process of cell migration towards the material.

3.4. Calcium-mediated osteopontin secretion by BM-rMSCs is one of the main signaling cues determining rEPCs recruitment in the microfluidic 3D assay

Based on the previously presented results, we decided to further study the role of OPN in the recruitment of rEPCs, as its role in this process is widely unknown. To test the hypothesis of OPN-mediated EPCs' recruitment, we performed a migration assay in coculture conditions treating the calcium-conditioned media with an OPN inhibitor (anti-OPN antibody at 10 µg/ml). We validated the use of this strategy by checking that osteopontin levels in cell culture media were significantly increased when the cells were stimulated with high levels of extracellular calcium salt for two days but drastically reduced when treated with the inhibitor (see Fig. 7-c). Regarding rEPCs migratory activity (see Fig. 7-a-b), the travelled migrated distance in calcium-treated media (104.3 ± 12.7 µm) was significantly higher than in the control condition (47.3 ± 5.0 µm) but drastically reduced when the anti-OPN antibody was added to the media (72.3 ± 12.1 µm). A decrease in the number of migrated cells was also observed when using the OPN inhibitor, from 58 ± 5 to 35 ± 4, being this value still higher than the one obtained in the control condition (23 ± 4 cells). These results are in line with several studies showing that the use of an anti-OPN antibody resulted in significant inhibition of angiogenesis in two different *in vivo* models (chick chorioallantoic membrane and corneal pocket assays), slowing down tumor progression [61]. Overall, our results suggest that calcium is not acting as a primary signal in rEPCs re-

cruitment, but rather as a mediator in the secretion of chemotactic proteins by rBM-rMSCs. Among the secreted chemotactic proteins, we found that osteopontin may play an important role in the migration events of rEPCs. This supports the idea that the crosstalk between rEPCs and BM-rMSCs is essential for the modulation of vascularization in bone healing [63,64] and that vasculogenesis and osteogenesis are closely linked [65]. Further studies should be performed to shed light on whether other key signals are also involved in the behavior of endothelial cells in angiogenic processes through cell crosstalking.

4. Conclusions

In this work, a novel 3D microfluidic assay to study the effects of calcium release on the recruitment of rEPCs is presented. We validated the functionality of the platform by evaluating the migration and proliferation in 3D of the two main cell types involved in this process (BM-rMSCs and rEPCs, both derived from rat bone marrow), and the possibility to generate gradients of bioactive molecules using an experimentally-validated finite element model. We also confirmed the possibility to incorporate and study calcium-releasing scaffolds in the platform, showing a significant increase in rEPCs' recruitment when using a pro-angiogenic electrospun scaffold made of PLA with calcium phosphate nanoparticles with respect to regular PLA controls. We also evidenced the utility of the assay to evaluate signaling cues involved in rEPCs' recruitment by studying the role of osteopontin in this process. The obtained results point to the central role of this protein in the calcium-mediated recruitment of rEPCs. Overall, we believe that the presented platform is an effective tool to evaluate and better understand the capacity of implant material candidates to recruit endogenous endothelial progenitors, a key step in the scaffold vascularization process.

Associated supplementary material

The supplementary material associated with this manuscript describes the procedure used to obtain the microfluidic mold, calculate the computational finite element model of the generated calcium gradient in our device and several properties of the proangiogenic material used in this study.

Declaration of Competing Interest

The authors declare that they have no known competing financial interests or personal relationships that could have appeared to influence the work reported in this paper.

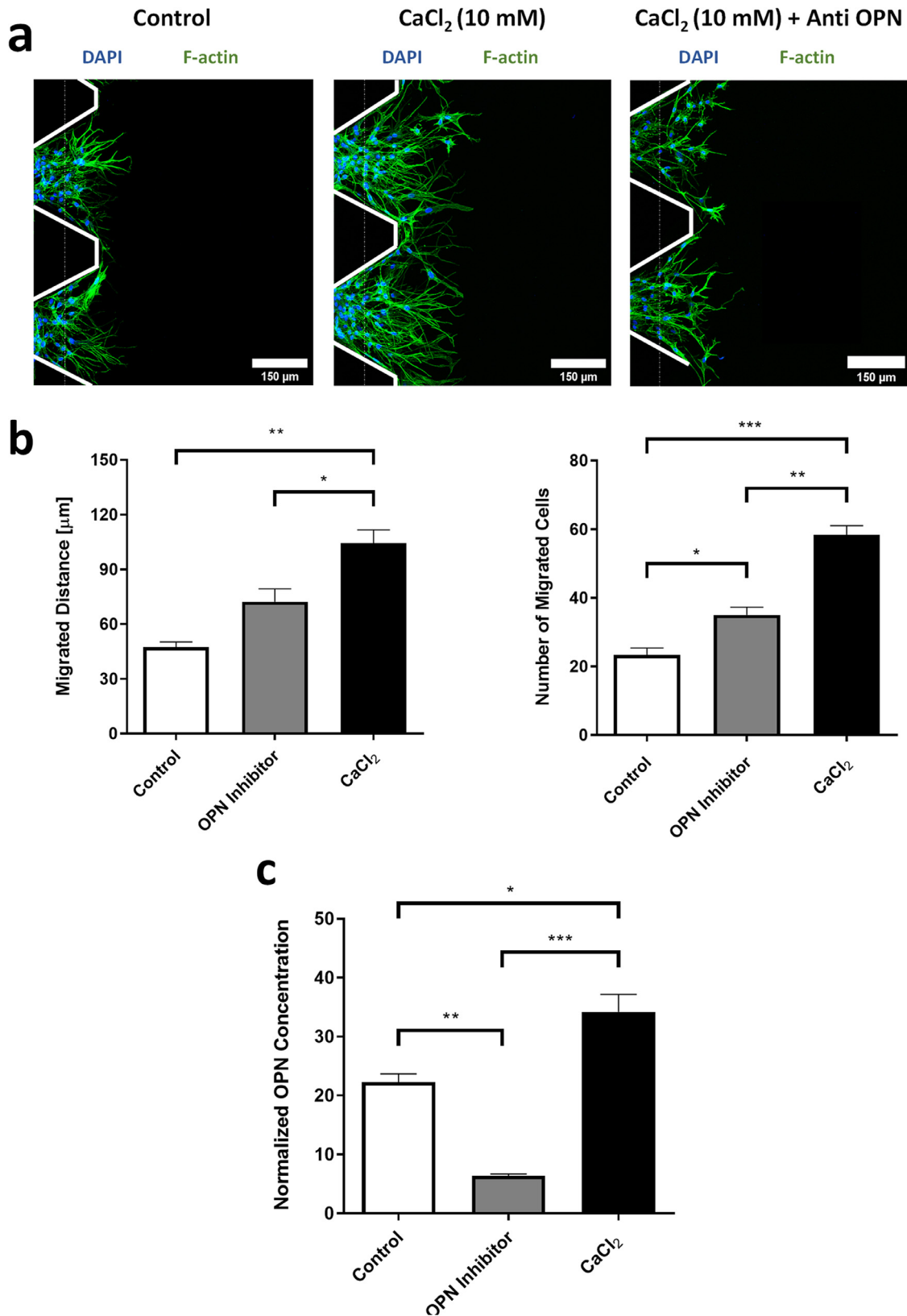The authors declare no competing financial interest.

Fig. 7. Evaluation of the osteopontin effect on rEPC migration in 3D microfluidic assay. (a) Confocal images of rEPC migration in three conditions: media with no supplementation (control), media supplemented with $CaCl_2$ at 10 mM and media supplemented with $CaCl_2$ at 10 mM with an osteopontin inhibitor. Cells were stained for F-actin (green), and cell nuclei (blue) after a total of 3 days in culture. (b) Analysis of the mean migrated distance and mean number of migrated cells with respect to the half of the microposts width (dotted white line in the microscopy images). (c) Total amount of osteopontin released by BM-rMSC 3D-cultured in the microfluidic devices for 3 days. Results are expressed as mean ± standard deviation ($n = 3$) with $^*p < 0.05$, $^{**}p < 0.01$ and $^*p < 0.001$ (evaluated with Student's *t*-test).

stitute of Barcelona (IBMB) for her advice and training on microscopy, David Izquierdo Garcia from the MicroFabSpace of the Institute for Bioengineering of Catalonia (IBEC) for his advice and training in microfabrication, and Adrianna Glinkowska Mares from the Nanoscopy for Nanomedicine at IBEC for her availability and valuable advice on microfluidics.

Supplementary materials

Supplementary material associated with this article can be found, in the online version, at doi:10.1016/j.actbio.2022.08.019.

References

[1] O. Demontiero, C. Vidal, G. Duque, Aging and bone loss: new insights for the clinician, Ther. Adv. Musculoskelet. Dis. 4 (2012) 61–76, doi:10.1177/1759720X11430858.

[2] C.E. Schwartz, J.F. Martha, P. Kowalski, D.A. Wang, R. Bode, L. Li, D.H. Kim, Prospective evaluation of chronic pain associated with posterior autologous iliac crest bone graft harvest and its effect on postoperative outcome, Health Qual. Life Outcomes 7 (2009), doi:10.1186/1477-7525-7-49.

[3] N.E.E. Xu, Bone-graft harvesting from iliac and fibular donor sites: techniques and complications, J. Am. Acad. Orthop. Surg. 9 (2001) 210–218.

[4] C. Delloye, O. Cornu, V. Druez, O. Barbier, Bone allografts, What they can offer and what they cannot, J. Bone Jt. Surg. Ser. B 89 (2007) 574–579, doi:10.1302/0301-620X.89B5.19039.

[5] G.M. Calori, E. Mazza, M. Colombo, C. Ripamonti, The use of bone-graft substitutes in large bone defects: any specific needs? Injury 42 (2011) S56–S63, doi:10.1016/j.injury.2011.06.011.

[6] W. Wang, K.W.K. Yeung, Bone grafts and biomaterials substitutes for bone defect repair: a review, Bioact. Mater. 2 (2017) 224–247, doi:10.1016/j.bioactmat.2017.05.007.

[7] P. Habibovic, K. de Groot, Osteoinductive biomaterials—properties and relevance in bone repair, J. Tissue Eng. Regen. Med. 1 (2007) 25–32, doi:10.1002/term.5.

[8] P.V. Giannoudis, T.A. Einhorn, G. Schmidmaier, D. Marsh, The diamond concept - open questions, Injury 39 (2008) S5, doi:10.1016/S0020-1383(08)70010-X.

[9] M. Sukul, T.B.L. Nguyen, Y.K. Min, S.Y. Lee, B.T. Lee, Effect of local sustainable release of BMP2-VEGF from nano-cellulose loaded in sponge biphasic calcium phosphate on bone regeneration, Tissue Eng. Part A. 21 (2015) 1822–1836, doi:10.1089/ten.tea.2014.0497.

[10] E. Wernike, M.O. Montjovent, Y. Liu, D. Wismeijer, E.B. Hunziker, K.A. Siebenrock, W. Hofstetter, F.M. Klenke, Vegf incorporated into calcium phosphate ceramics promotes vascularisation and bone formation *in vivo*, Eur. Cells Mater. 19 (2010) 30–40, doi:10.22203/ecm.v019a04.

[11] A. Minamide, M. Yoshida, M. Kawakami, M. Okada, Y. Enyo, H. Hashizume, S.D. Boden, The effects of bone morphogenetic protein and basic fibroblast growth factor on cultured mesenchymal stem cells for spine fusion, Spine 32 (2007) 1067–1071 (Phila. Pa. 1976, doi:10.1097/01.brs.0000261626.32999.8a.

[12] K.S. Moon, E.J. Choi, S. Oh, S. Kim, The effect of covalently immobilized FGF-2 on biphasic calcium phosphate bone substitute on enhanced biological compatibility and activity, (2015). 10.1155/2015/742192.

[13] F.R. Formiga, E. Tamayo, T. Simón-Yarza, B. Pelacho, F. Prósper, M.J. Blanco-Prieto, Angiogenic therapy for cardiac repair based on protein delivery systems, Heart Fail. Rev. 17 (2012) 449–473, doi:10.1007/s10741-011-9285-8.

[14] O. Castaño, S. Pérez-Amodio, C. Navarro-Requena, M.Á. Mateos-Timoneda, E. Engel, Instructive microenvironments in skin wound healing: biomaterials as signal releasing platforms, Adv. Drug Deliv. Rev. 129 (2018), doi:10.1016/j.addr.2018.03.012.

[15] A.M. Hofer, Another dimension to calcium signaling: a look at extracellular calcium, J. Cell Sci. 118 (2005) http://jcs.biologists.org/content/118/5/855.long. accessed July 10, 2017.

[16] D. Goltzman, G.N. Hendy, The calcium-sensing receptor in bone-mechanistic and therapeutic insights, Nat. Rev. Endocrinol. 11 (2015) 298–307, doi:10.1038/nrendo.2015.30.

[17] A. Aguirre, A. González, M. Navarro, O. Castaño, J.A. Planell, E. Engel, Control of microenvironmental cues with a smart biomaterial composite promotes endothelial progenitor cell angiogenesis, Eur. Cells Mater. 24 (2012) 90–106.

[18] H. Oliveira, S. Catros, C. Boiziau, R. Siadous, J. Marti-Munoz, R. Bareille, S. Rey, O. Castano, J. Planell, J. Amédée, E. Engel, The proangiogenic potential of a novel calcium releasing biomaterial: impact on cell recruitment, Acta Biomater. 29 (2016) 435–445, doi:10.1016/j.actbio.2015.10.003.

[19] O. Castaño, N. Sachot, E. Xuriguera, E. Engel, J.A. Planell, J.H. Park, G.Z. Jin, T.H. Kim, J.H. Kim, H.W. Kim, Angiogenesis in bone regeneration: tailored calcium release in hybrid fibrous scaffolds, ACS Appl. Mater. Interfaces. 6 (2014) 7512–7522, doi:10.1021/am500885v.

[20] C. Sandino, S. Checa, P.J. Prendergast, D. Lacroix, Simulation of angiogenesis and cell differentiation in a CaP scaffold subjected to compressive strains using a lattice modeling approach, Biomaterials 31 (2010) 2446–2452, doi:10.1016/j.biomaterials.2009.11.063.

[21] N.F. Jufri, A. Mohamedali, A. Avolio, M.S. Baker, Mechanical stretch: physiological and pathological implications for human vascular endothelial cells, Vasc. Cell. 7 (2015), doi:10.1186/s13221-015-0033-z.

[22] F. Bai, Z. Wang, J. Lu, J. Liu, G. Chen, R. Lv, J. Wang, K. Lin, J. Zhang, X. Huang, The correlation between the internal structure and vascularization of controllable porous bioceramic materials *in vivo*: a quantitative study, Tissue Eng. Part A 16 (2010) 3791–3803, doi:10.1089/ten.tea.2010.0148.

[23] B. Feng, Z. Jinkang, W. Zhen, L. Jianxi, C. Jiang, M. Guolin, D. Xin, The effect of pore size on tissue ingrowth and neovascularization in porous bioceramics of controlled architecture *in vivo*, Biomed. Mater. 6 (2011) 15007, doi:10.1088/1748-6041/6/1/015007.

[24] F.M. Klenke, Y. Liu, H. Yuan, E.B. Hunziker, K.A. Siebenrock, W. Hofstetter, Impact of pore size on the vascularization and osseointegration of ceramic bone substitutes *in vivo*, J. Biomed. Mater. Res. Part A 85 (2008) 777–786, doi:10.1002/jbm.a.31559.

[25] G.A. Van Norman, Limitations of animal studies for predicting toxicity in clinical trials: is it time to rethink our current approach? JACC Basic Transl. Sci. 4 (2019) 845–854, doi:10.1016/j.jacbts.2019.10.008.

[26] A.D. Van Der Meer, A. Van Den Berg, Organs-on-chips: breaking the *in vitro* impasse, Integr. Biol. 4 (2012) 461–470, doi:10.1039/c2ib00176d.

[27] S.N. Bhatia, D.E. Ingber, Microfluidic organs-on-chips, Nat. Biotechnol. 32 (2014) 760–772, doi:10.1038/nbt.2989.

[28] A. López-Canosa, S. Perez-Amodio, E. Yanac-Huertas, J. Ordoño, R. Rodriguez-Trujillo, J. Samitier, O. Castaño, E. Engel, A microphysiological system combining electrospun fibers and electrical stimulation for the maturation of highly anisotropic cardiac tissue, Biofabrication 13 (2021), doi:10.1088/1758-5090/abff12.

[29] S. Kim, H. Lee, M. Chung, N.L. Jeon, Engineering of functional, perfusable 3D microvascular networks on a chip, Lab Chip 13 (2013) 1489–1500, doi:10.1039/c3lc41320a.

[30] S. Kim, M. Chung, J. Ahn, S. Lee, N.L. Jeon, Interstitial flow regulates the angiogenic response and phenotype of endothelial cells in a 3D culture model, Lab Chip 16 (2016) 4189–4199, doi:10.1039/c6lc00910g.

[31] Y. Shin, J.S. Jeon, S. Han, G.S. Jung, S. Shin, S.H. Lee, R. Sudo, R.D. Kamm, S. Chung, *In vitro* 3D collective sprouting angiogenesis under orchestrated ANG-1 and VEGF gradients, Lab Chip 11 (2011) 2175–2181, doi:10.1039/c1lc20039a.

[32] Y. Shin, S. Han, J.S. Jeon, K. Yamamoto, I.K. Zervantonakis, R. Sudo, R.D. Kamm, S. Chung, Microfluidic assay for simultaneous culture of multiple cell types on surfaces or within hydrogels, Nat. Protoc. 7 (2012) 1247–1259, doi:10.1038/nprot.2012.051.

[33] S.L. Natividad-Diaz, S. Browne, A.K. Jha, Z. Ma, S. Hossainy, Y.K. Kurokawa, S.C. George, K.E. Healy, A combined hiPSC-derived endothelial cell and *in vitro* microfluidic platform for assessing biomaterial-based angiogenesis, Biomaterials 194 (2019) 73–83, doi:10.1016/j.biomaterials.2018.11.032.

[34] J. Bai, K. Haase, J.J. Roberts, J. Hoffmann, H.T. Nguyen, Z. Wan, S. Zhang, B. Sarker, N. Friedman, Č. Ristić-Lehmann, R.D. Kamm, A novel 3D vascular assay for evaluating angiogenesis across porous membranes, Biomaterials 268 (2021) 120592, doi:10.1016/j.biomaterials.2020.120592.

[35] A. Aguirre, A. González, J.A. Planell, E. Engel, Extracellular calcium modulates *in vitro* bone marrow-derived Flk-1$^+$ CD34$^+$ progenitor cell chemotaxis and differentiation through a calcium-sensing receptor, Biochem. Biophys. Res. Commun. (2010) 393, doi:10.1016/j.bbrc.2010.01.109.

[36] A. González-Vázquez, J.A. Planell, E. Engel, Extracellular calcium and CaSR drive osteoinduction in mesenchymal stromal cells, Acta Biomater. 10 (2014) 2824–2833, doi:10.1016/j.actbio.2014.02.004.

[37] A.Y. Khakoo, T. Finkel, Endothelial progenitor cells, Annu. Rev. Med. 56 (2005) 79–101, doi:10.1146/ANNUREV.MED.56.090203.104149.

[38] R.E. Favoni, A. De Cupis, The role of polypeptide growth factors in human carcinomas: new targets for a novel pharmacological approach, Pharmacol. Rev. 52 (2000) 179–206.

[39] I.A. Silver, R.J. Murrills, D.J. Etherington, Microelectrode studies on the acid microenvironment beneath adherent macrophages and osteoclasts, Exp. Cell Res. 175 (1988) 266–276, doi:10.1016/0014-4827(88)90191-7.

[40] A. Aguirre, A. González, J.A. Planell, E. Engel, Extracellular calcium modulates *in vitro* bone marrow-derived Flk-1+ CD34+ progenitor cell chemotaxis and differentiation through a calcium-sensing receptor, Biochem. Biophys. Res. Commun. 393 (2010) 156–161, doi:10.1016/j.bbrc.2010.01.109.

[41] J. Braga, J.M.P. Desterro, M. Carmo-Fonseca, Intracellular macromolecular mobility measured by fluorescence recovery after photobleaching with confocal laser scanning microscopes, Mol. Biol. Cell. 15 (2004) 4749–4760, doi:10.1091/mbc.E04-06-0496.

[42] I. Zervantonakis, S. Chung, R. Sudo, M. Zhang, J. Charest, R. Kamm, Concentration gradients in microfluidic 3D matrix cell culture systems, Int. J. Micro-Nano Scale Transp. 1 (2010) 27–36, doi:10.1260/1759-3093.1.1.27.

[43] C.L.E. Helm, M.E. Fleury, A.H. Zisch, F. Boschetti, M.A. Swartz, Synergy between interstitial flow and VEGF directs capillary morphogenesis *in vitro* through a gradient amplification mechanism, Proc. Natl. Acad. Sci. U. S. A. 102 (2005) 15779–15784, doi:10.1073/pnas.0503681102.

[44] E.S. Sanzana, M. Navarro, F. Macule, S. Suso, J.A. Planell, M.P. Ginebra, Of the *in vivo* behavior of calcium phosphate cements and glasses as bone substitutes, Acta Biomater. 4 (2008) 1924–1933, doi:10.1016/j.actbio.2008.04.023.

[45] J. Schindelin, I. Arganda-Carreras, E. Frise, V. Kaynig, M. Longair, T. Pietzsch, S. Preibisch, C. Rueden, S. Saalfeld, B. Schmid, J.Y. Tinevez, D.J. White, V. Hartenstein, K. Eliceiri, P. Tomancak, A. Cardona, Fiji: an open-source platform for biological-image analysis, Nat. Methods 9 (2012) 676–682, doi:10.1038/nmeth.2019.

[46] S. Bolte, F.P. Cordelières, A guided tour into subcellular colocalization analysis in light microscopy, J. Microsc. 224 (2006) 213–232, doi:10.1111/j.1365-2818.2006.01706.x.

[47] G. Schuszter, T. Gehér-Herczegh, Á. Szucs, Á. Tóth, D. Horváth, Determination of the diffusion coefficient of hydrogen ion in hydrogels, Phys. Chem. Chem. Phys. 19 (2017) 12136–12143, doi:10.1039/c7cp00986k.

[48] S.H. Lim, C. Kim, A.R. Aref, R.D. Kamm, M. Raghunath, Complementary effects of ciclopirox olamine, a prolyl hydroxylase inhibitor and sphingosine 1-phosphate on fibroblasts and endothelial cells in driving capillary sprouting, Integr. Biol. 5 (2013) 1474–1484 (United Kingdom), doi:10.1039/c3ib40082d.

[49] M. Ishii, M. Takahashi, J. Murakami, T. Yanagisawa, M. Nishimura, Vascular endothelial growth factor-C promotes human mesenchymal stem cell migration via an ERK-and FAK-dependent mechanism, Mol. Cell. Biochem. 455 (2019) 185–193, doi:10.1007/s11010-018-3481-y.

[50] A. De Donatis, F. Ranaldi, P. Cirri, Reciprocal control of cell proliferation and migration, Cell Commun. Signal. 8 (2010) 1–4, doi:10.1186/1478-811X-8-20/FIGURES/1.

[51] M.N. Lee, H.S. Hwang, S.H. Oh, A. Roshanzadeh, J.W. Kim, J.H. Song, E.S. Kim, J.T. Koh, Elevated extracellular calcium ions promote proliferation and migration of mesenchymal stem cells via increasing osteopontin expression, Exp. Mol. Med. 50 (2018), doi:10.1038/s12276-018-0170-6.

[52] E.W. Esch, A. Bahinski, D. Huh, Organs-on-chips at the frontiers of drug discovery, Nat. Rev. Drug Discov. 14 (2015) 248–260, doi:10.1038/nrd4539.

[53] A.K. Olsson, A. Dimberg, J. Kreuger, L. Claesson-Welsh, VEGF receptor signalling - in control of vascular function, Nat. Rev. Mol. Cell Biol. 7 (2006) 359–371, doi:10.1038/NRM1911.

[54] S.P. Yun, M.Y. Lee, J.M. Ryu, C.H. Song, H.J. Han, Role of HIF-1alpha and VEGF in human mesenchymal stem cell proliferation by 17beta-estradiol: involvement of PKC, PI3K/Akt, and MAPKs, Am. J. Physiol. Cell Physiol. 296 (2009), doi:10.1152/AJPCELL.00415.2008.

[55] S.Y. Tan, Z. Leung, A.R. Wu, Recreating physiological environments *in vitro*: design rules for microfluidic-based vascularized tissue constructs, Small 16 (2020) 1905055, doi:10.1002/smll.201905055.

[56] B. Zhang, A. Korolj, B.F.L. Lai, M. Radisic, Advances in organ-on-a-chip engineering, Nat. Rev. Mater. 3 (2018) 257–278, doi:10.1038/s41578-018-0034-7.

[57] K. Joensuu, L. Uusitalo-Kylmälä, T.A. Hentunen, T.J. Heino, Angiogenic potential of human mesenchymal stromal cell and circulating mononuclear cell cocultures is reflected in the expression profiles of proangiogenic factors leading to endothelial cell and pericyte differentiation, J. Tissue Eng. Regen. Med. 12 (2018) 775–783, doi:10.1002/term.2496.

[58] T.P. Lozito, C.K. Kuo, J.M. Taboas, R.S. Tuan, Human mesenchymal stem cells express vascular cell phenotypes upon interaction with endothelial cell matrix, J. Cell. Biochem. 107 (2009) 714–722, doi:10.1002/jcb.22167.

[59] Y.S. Maeng, H.J. Choi, J.Y. Kwon, Y.W. Park, K.S. Choi, J.K. Min, Y.H. Kim, P.G. Suh, K.S. Kang, M.H. Won, Y.M. Kim, Y.G. Kwon, Endothelial progenitor cell homing: prominent role of the IGF2-IGF2R-PLC 22 axis, Blood 113 (2009) 233–243, doi:10.1182/blood-2008-06-162891.

[60] J. Chen, K. Singh, B.B. Mukherjee, J. Sodek, Developmental expression of osteopontin (OPN) mRNA in rat tissues: evidence for a role for OPN in bone formation and resorption, Matrix 13 (1993) 113–123, doi:10.1016/s0934-8832(11)80070-3.

[61] H. Zhao, Q. Chen, A. Alam, J. Cui, K.C. Suen, A.P. Soo, S. Eguchi, J. Gu, D. Ma, The role of osteopontin in the progression of solid organ tumour, Cell Death Dis. 9 (2018) 356, doi:10.1038/s41419-018-0391-6.

[62] J. Dai, L. Peng, K. Fan, H. Wang, R. Wei, G. Ji, J. Cai, B. Lu, B. Li, D. Zhang, Y. Kang, M. Tan, W. Qian, Y. Guo, Osteopontin induces angiogenesis through activation of PI3K/AKT and ERK1/2 in endothelial cells, Oncogene 28 (2009) 3412–3422, doi:10.1038/onc.2009.189.

[63] A. Aguirre, J.A. Planell, E. Engel, Dynamics of bone marrow-derived endothelial progenitor cell/mesenchymal stem cell interaction in co-culture and its implications in angiogenesis, Biochem. Biophys. Res. Commun. 400 (2010) 284–291 10.1016/j.bbrc.2010.08.073.

[64] J. Rouwkema, P.E. Westerweel, J. De Boer, M.C. Verhaar, C.A. Van Blitterswijk, The use of endothelial progenitor cells for prevascularized bone tissue engineering, Tissue Eng. Part A 15 (2009) 2015–2027, doi:10.1089/ten.tea.2008.0318.

[65] K.D. Hankenson, M. Dishowitz, C. Gray, M. Schenker, Angiogenesis in bone regeneration, Injury 42 (2011) 556–561, doi:10.1016/j.injury.2011.03.035.